Macromolecular Research, Vol. 17, No. 9, pp 638-645 (2009)

# Microstructure and Properties of Fully Aliphatic Polyimide/Mesoporous Silica Hybrid Composites

**Anu Stella Mathews†, Yuin Jung, Taesung Lee, Sung Soo Park, Il Kim, and Chang-Sik Ha***

*Department of Polymer Science and Engineering, Pusan National University, Busan 609-735, Korea*

**M. Selvaraj**

*Department of Chemical Engineering, Pusan National University, Busan 609-735, Korea*

**Mijeong Han**

*Advanced Materials Division, Korea Research Institute of Chemical Technology, Daejeon 305-600, Korea*

*Received October 20, 2008; Revised November 14, 2008; Accepted November 14, 2008*

**Abstract:** We report the effect of the amount of the mesoporous material, SBA-15, on the basic traits of fully aliphatic polyimides (API). For this purpose, water soluble, fully aliphatic poly(amic acid) triethyl amine salts ($PAA_{(s)}$) were prepared and mixed with various amounts of SBA-15. Fully aliphatic polyimide hybrid composites containing the SBA 15-type mesoporous silica were synthesized successfully from bicyclo [2.2.2] oct-7-ene-2,3,5,6-tetracarboxylic dianhydride and alicyclic diamine, 4,4'-methylene bis(2-methylcyclohexylamine). The structure of the hybrid composites was confirmed by IR spectroscopic analysis. Scanning electron microscopy revealed the morphology of the compounds. The hybrid composites exhibited good thermal stability, reasonable transparency, and a low dielectric constant.

*Keywords:* hybrid composites, fully aliphatic polyimides, mesoporous silica, dielectric properties.

## Introduction

Mesoporous materials are a special type of nano-materials with ordered arrays of uniform nano-channels. The well-known, potentially useful catalytic, magnetic, optical and semiconducting properties of silica based mesoporous materials have been exploited in various technological and biomedical applications.[1,2] SBA-15 is a typical mesoporous material with large pore size and which has highly ordered two dimensional hexagonally arranged meso-channels, with thick walls, an adjustable pore size from 3 to 30 nm, and high hydrothermal and thermal stability.[3] Therefore, SBA-15 is a promising material, particularly for reactions occurring at high temperatures[4,5] and has also been used as a low dielectric constant ($\varepsilon$) material.[6]

Polyimides are one of the most important classes of polymers widely used in the microelectronics and photoelectronics industries owing to their high thermal stability and chemical resistance and their good mechanical and electric properties.[7] Although aromatic polyimides possess excellent properties, there are a number of obstacles that hinder the extension of their applications to opto-electronic materials and high-speed multilayer printed wiring boards, such as their insolubility in common solvents in their fully imidized form, the light or dark-yellow color of their films caused by intra- and intermolecular charge transfer (CT) interactions, and their high dielectric constants. In this sense, fully aliphatic and alicyclic polyimides (API) are currently being considered for applications in optoelectronics and interlayer dielectric materials, because of their higher transparencies and lower dielectric constants,[8-10] which result from their low molecular density and polarity and the low probability of their undergoing inter- or intramolecular charge transfer.

In this era of emerging hybrid composite materials, the hybrid composites of API and SBA-15 mesoporous compounds constitute a new avenue of investigation. In this work, therefore, we report the preparation and characterization of novel API / SBA-15 hybrid composites. The water soluble polyimide precursor, polyamic acid triethyl amine salt ($PAA_{(s)}$) and mesoporous materials are imidized in water to obtain the desired API/SBA-15 hybrid composites. Varying ratios of SBA-15 and APIs are used to optimize the trans-

*Corresponding Author. E-mail: csha@pnu.edu

†Present address; Alberta Lipid Utilization Research Program, Department of Agricultural, Food and Nutritional Science, University of Alberta, Edmonton, Alberta, Canada.

parence, thermal stability and dielectric constant of the hybrid composites. To the best of knowledge, this is the first attempt to use fully aliphatic polyimides for making mesoporous hybrid composite materials and water soluble precursor intermediates and this constitutes the novelty of the present study.

## Experimental

**Materials.** All reagents and chemicals were purchased from Aldrich Chemical Company. Bicyclo [2.2.2] oct-7-ene 2,3,5,6-tetra carboxylic dianhydride (BOCA) was recrystallized from acetic anhydride and dried at 150 °C under a vacuum before use. The cycloaliphatic diamines, 4,4'-methylene bis(2-methyl cyclohexylamine) (MMCA), was distilled under reduced pressure. Triethyl amine (TEA) was used as received. *N*-Methyl pyrrolidone (NMP) was dried with calcium hydride and vacuum distilled before use. All chemicals were stored and handled under a nitrogen atmosphere in a glove box.

**Preparation of Polyamic Acid Salts ($PAA_{(s)}$).** 5 mmols of diamine was dissolved in NMP and to this solution 5 mmols of BOCA was added at room temperature and stirred for 24 h to obtain homogeneous viscous polyamic acid (PAA). The PAA was obtained from BOCA and MMCA. The $PAA_{(s)}$ was prepared by adding 10 mmol of TEA dropwise to the viscous PAA solution. Upon the addition of TEA, a large increase in viscosity was observed along with a local white precipitate of the polymer. After stirring half an hour, it became a homogeneous solution, indicating the formation of water soluble polyamic acids.[11,12] The solution was poured into acetone and the precipitated solid was filtered and dried in a vacuum. Scheme I represents the synthesis procedure.

**Preparation of Mesoporous Silica SBA-15.** In a typical synthesis,[13] 16 g of the triblock copolymer, poly(ethylene oxide)-*block*-poly(propylene oxide)-*block*-poly(ethylene oxide) ($PEO_{20}PPO_{70}PEO_{20}$ : P123, $M_n$=5,800), was dissolved in 500 g of water and 80 g of 35 wt% HCl with stirring at 35 °C until a homogeneous solution was obtained. Then, 34.4 g of tetraethoxysilane (TEOS) was added to this homogeneous solution, the mixture stirred for 15 min and then allowed to react for 24 h under static conditions at the same temperature. Subsequently, the mixture was aged at 100 °C for an additional 24 h. The resulting solid product was collected by filtration, washed thoroughly with water repeatedly and dried at 80 °C. The as-synthesized sample was heated from room temperature to 550 °C at a rate of 1 °C/min and was kept at 550 °C for 4 h in a furnace under air for removing template.

**Preparation of API/SBA-15 Hybrid Composites.** Varying amounts of the SBA-15 mesoporous materials synthesized for this work were dissolved in 5 mL of distilled water containing 2 wt% TEA by sonicating the solution for 1 h. To this solution, 0.26 g of the synthesized $PAA_{(s)}$ powders

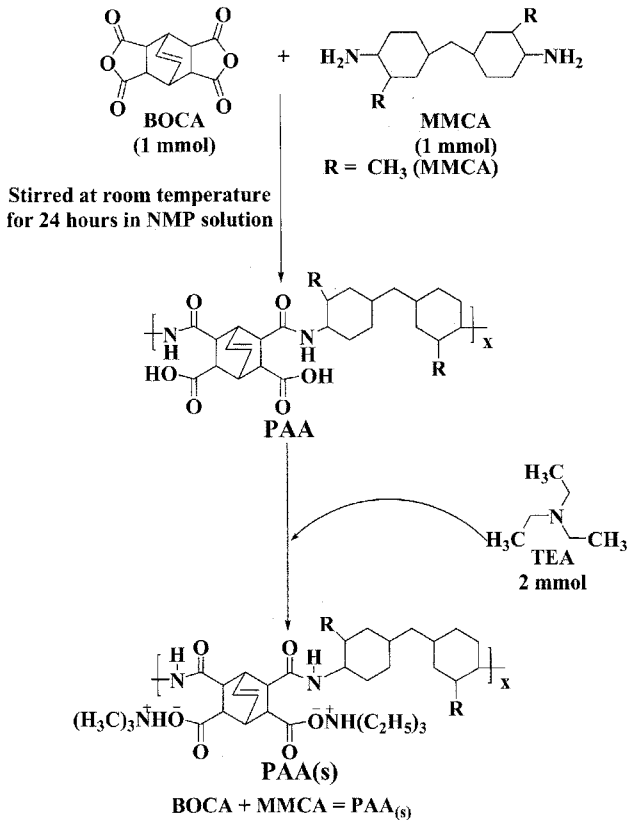


**Scheme I.** Synthesis of water soluble poly(amic acid) triethyl amine salt precursors.

were added and stirred for 24 h to obtain the $PAA_{(s)}$/SBA-15 hybrid composite solutions. These solutions were finally subjected to stepwise thermal imidization to yield the API/SBA-15 hybrid composites.

**Film Casting.** The PAA/SBA-15 hybrid composite solution in water was poured into a Petri dish and heated in a vacuum oven at 30 °C for 12 h, 60 °C for 6 h, 80 °C for 3 h and 150 °C for 1 h. Then, the baked films were transferred to a nitrogen atmosphere and the temperature was raised to 200 °C for 1 h, 250 °C, 300 °C and 350 °C for 30 min each and then slowly cooled to room temperature to obtain the API/SBA-15 hybrid composite films. To carry out the dielectric constant and transparency measurements, solutions of the APIs prior to their precipitation were spin coated onto clean ITO glass and quartz plates, respectively, and submitted to the heating cycle described above. The series of polymer hybrid composites synthesized in this work are listed in Table I.

**Measurements.** The infrared spectra (KBr disks) were recorded on a Shimadzu IR Prestige-21. The $^1H$ and $^{13}C$ NMR spectra were recorded on a Varian Unity Plus-300 (300 MHz) NMR spectrometer. The thermogravimetric analysis (TGA) was performed under nitrogen on a TGA Q50 Q Series thermal analyzer. The sample was heated at a heating rate of 10 °C/min from 50 to 600 °C. Differential scanning calorim-

etry (DSC) was conducted under $N_2$ with a TA instruments Q 100 DSC. The sample was heated at 20 °C/min from 50 to 500 °C. The optical properties were measured from the ultraviolet-visible spectra recorded from one accumulation on a HITACHI U-2010 spectrometer. The dielectric constant was obtained at 1 MHz from the formula $K=C\cdot d/A\varepsilon_o$, where $C$ is the capacitance observed using an impedance-gain phase analyzer (HP4194A), $d$ is the film thickness (each film was 1.0 ± 0.05 μm thick), $A$ is the area, and $\varepsilon_o$ is the free permittivity. The thicknesses of all of the thin films were measured using a surface profiler (KLA Tencor, Alpha-Step IQ). The SEM images of the samples were taken with a JEOL-FESEM (JSM-6700F). The wide-angle X-ray diffraction (WAXD) measurements of the pulverized samples were conducted at room temperature in reflection mode using a Rigaku diffractometer (Model Rigaku Miniflex). Small angle X-ray scattering (SAXS) was performed with Co-K$\alpha$ ($\lambda$= 1.608 Å) radiation with an energy range of 4-16 keV at the Pohang Accelerator Laboratory, Korea. The TEM images were recorded on a JEOL 2010 electron microscope operating at 200 kV. The BET (Brumauer-Emmett-Teller) method was used to calculate the specific surface area. The pore size distribution was calculated from the analysis of the desorption branch of the isotherm by the BJH (Barett-Joyner-Halenda) method.

## Results and Discussion

**Microstructure and Properties of Synthesized Mesoporous Silica.** The typical mesoporous silica material, SBA-15, was synthesized by using $PEO_{20}PPO_{70}PEO_{20}$ triblock copolymer as a template. Figure 1(a) shows the SAXS patterns of the calcined SBA-15, which exhibit five well resolved peaks, viz. three prominent peaks at 0.66, 1.15, and 1.33 $nm^{-1}$ and two weak peaks at 1.75 and 2.00 $nm^{-1}$, that can be indexed as the (100), (110), (200), (220) and (300) reflections of p6mm hexagonal symmetry with lattice d-spacings of 9.5, 5.5, 4.7, 3.6 and 3.1 nm, respectively.[14] The corresponding unit cell parameter, $a_0$, is 10.6 nm ($a_0=2d(100)/\sqrt{3}$). Figure 1(b) shows the mesopore properties of SBA-15 obtained from the nitrogen adsorption-desorption isotherms, which were identified as belonging to type IV according to the classification of Brunauer *et al.*,[15] with a reversible part and a type A hysteresis loop at high pressure. The synthesized SBA-15 has a pore diameter of 6.00 nm, and its surface area and total pore volume were calculated to be 618 $m^2/g$ and 0.9 $cm^3/g$, respectively. These parameters indicate the presence of some amount of air voids stored in the mesoporous silica materials.[16] The TEM images shown in Figure 2 are used to support the SAXS data regarding the structural information such as the mesophase symmetry and pore size of the synthesized SBA-15. The TEM image reveals that the samples possess a well ordered hexagonal array channel structure.

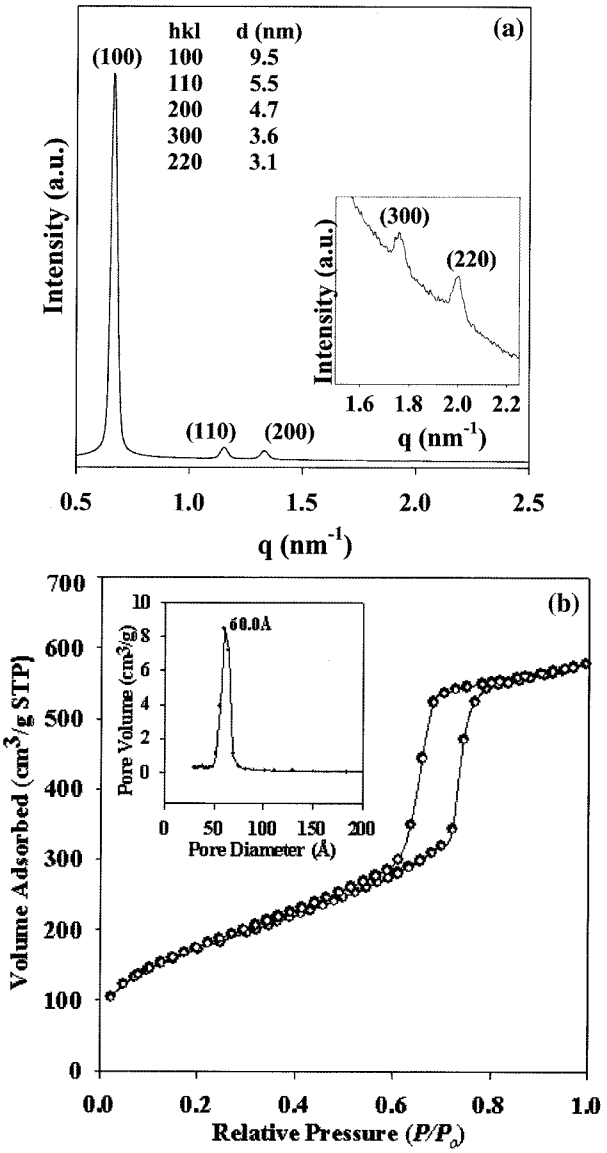


**Figure 1.** (a) Small angle X-ray scattering (SAXS) patterns and (b) Nitrogen adsorption-desorption isotherm for calcined SBA-15.

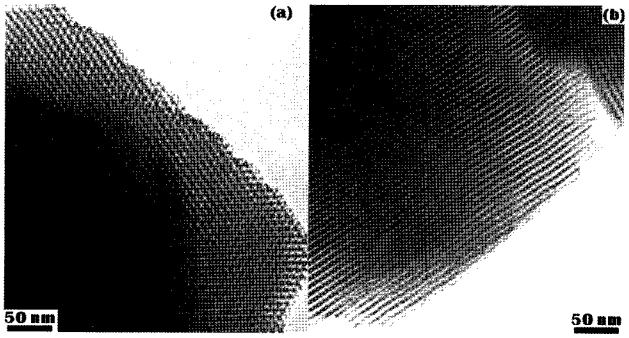


**Figure 2.** TEM images of calcined SBA-15 (a) [100] and (b) [110] zone axes.

**Structural Studies of PAA, $PAA_{(s)}$.** Figure 3 presents the FTIR spectra of the synthesized polyamic acids and poly

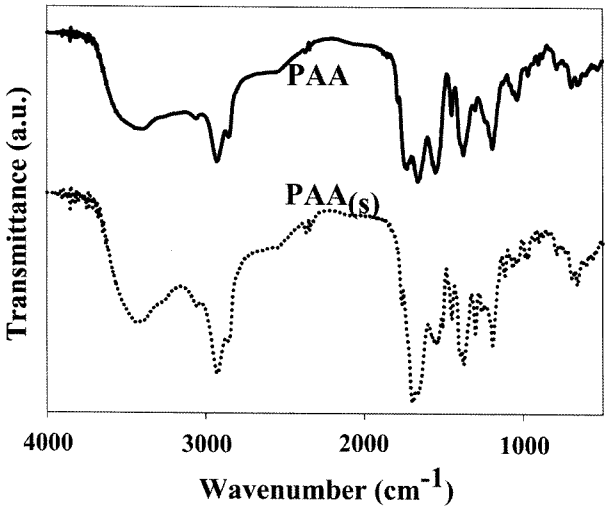


**Figure 3.** IR spectra of polyamic acids, PAA and poly(amic acid) triethyl amine salts, $PAA_{(s)}$.

(amic acid) triethyl amine salts. From the characteristic transmission peaks, such as those at 3295 $cm^{-1}$ for the amide stretching overlapped with the hydroxyl group transmission at 3200-3700 $cm^{-1}$, 1720 $cm^{-1}$ for the C=O (acid) stretching, 1660 $cm^{-1}$ for the C=O (amide) stretching, 1560 $cm^{-1}$ for the NH (amide) stretching, and 1310-1277 $cm^{-1}$ for the amide C-N bending, it was disclosed that the aliphatic polyamic acids were successfully synthesized by the reaction between the amines and BOCA.[17,18] The peaks of the $PAA_{(s)}$ samples were identical to those of PAA with the exception of a shift in the carboxylic acid peak position, due to the ionic interaction between the triethylamine moieties, thus proving the formation of the poly(amic acid) triethylamine salts, which was further confirmed using $^1H$ NMR spectroscopy.

Figure 4 shows the $^1H$ NMR spectra of the synthesized polyamic acid PAA and water soluble poly(amic acid) tri-

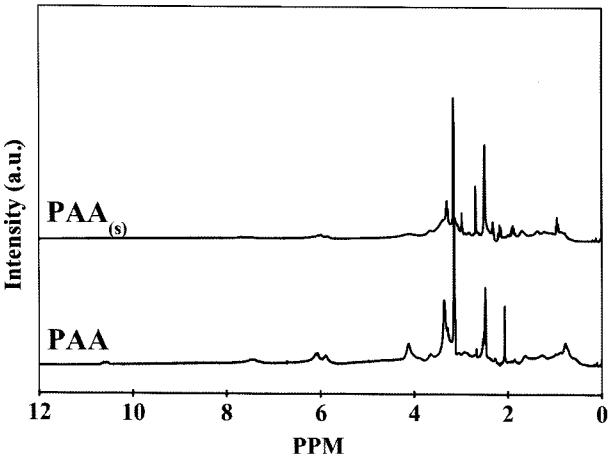


**Figure 4.** $^1H$ NMR spectra of polyamic acids, PAA, and poly(amic acid) triethyl amine salts, $PAA_{(s)}$.

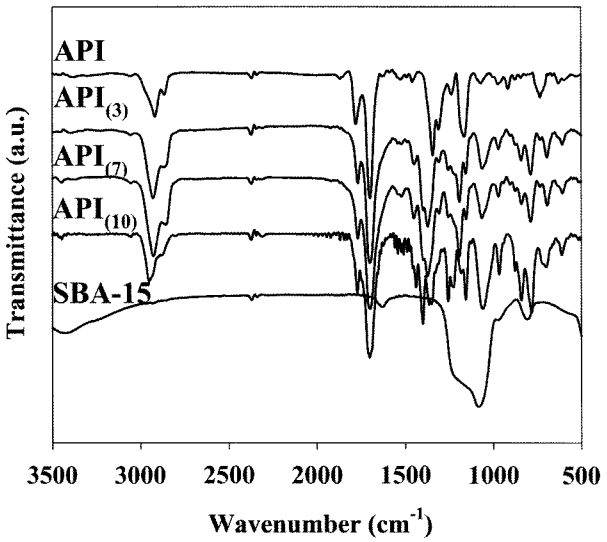


**Figure 5.** FTIR spectra of representative polyimide hybrid composites: $API_{(3)}$, $API_{(7)}$ and $API_{(10)}$, in comparison with those of pure API and SBA-15.

ethylamine salts, $PAA_{(s)}$. PAA showed the characteristic peaks as the spectra indicate. The -OH peak at around 11.0 ppm and -NH peak at 7.5 ppm prove the formation of polyamic acid. For $PAA_{(s)}$, the peaks of ethylene triamine appear at around 1.0-2.4 ppm and the -OH peak at 11.0 ppm is not present.

**Structural Confirmation of API/SBA-15 Hybrid Composites.** The compounds were characterized using FTIR spectra, as shown in Figure 5. We observed a number of typical, characteristic peaks, namely those at 1789 $cm^{-1}$ (C=O symmetric stretching), 1716 $cm^{-1}$ (C=O asymmetric stretching), 1375 $cm^{-1}$ (C-N-C stretching), and 739 $cm^{-1}$ (imide ring deformation), denoting the formation of the polyimide structure for all samples. The peaks at 1100 $cm^{-1}$ and 790 $cm^{-1}$ due to the asymmetric and symmetric stretching vibration modes of Si-O-Si, respectively, appeared for the hybrid composites, whose intensity relative to that of the polyimide peaks increased as the amount of SBA-15 increased in the hybrid composites.

**Morphology of Hybrid Composite Films.** Figure 6 shows the SEM images of the API/SBA 15 hybrid composite surfaces and that of pure API as a reference. The hybrid composite with a lower amount of SBA-15 showed uniformly well mixed particles in the polymer matrix, while increasing the amount of SBA-15 resulted in phase separation, eventually resulting in inorganic particle domains with a size of about 1 μm in the API matrix, as shown for the hybrid composite with 15 wt% of SBA 15 (Figure 6(f)).

**Thermal Stability and Phase Transitions.** The polymers underwent 5% weight loss within the temperature range of 308 to 431 °C and 10% weight loss between 364 to 444 °C. Figure 7 displays the TGA curves of the aliphatic polyim-

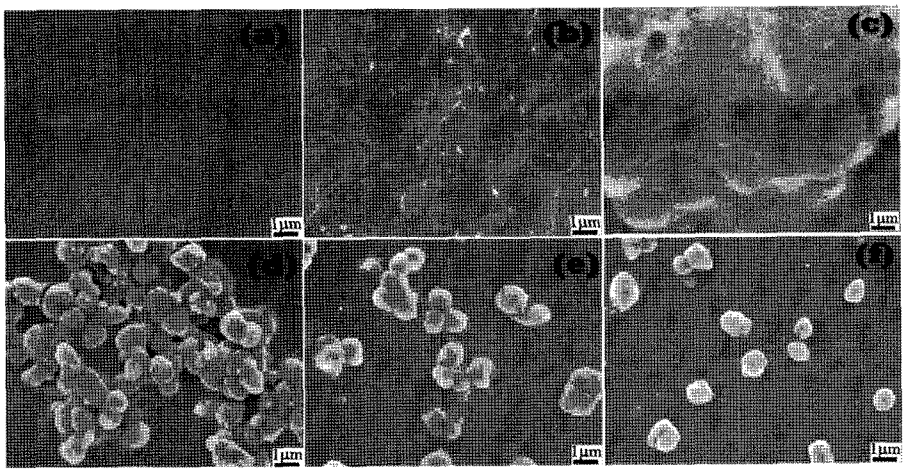

**Figure 6.** SEM images of the API/mesoporous silica hybrid composites: (a) API, (b) $API_{(3)}$, (c) $API_{(5)}$, (d) $API_{(7)}$, (e) $API_{(10)}$, and (f) $API_{(15)}$.

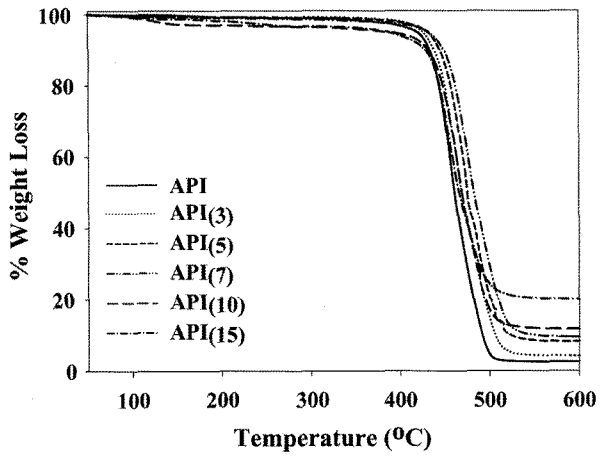


**Figure 7.** TGA thermograms of the pure API and its SBA-15 hybrid composites in $N_2$ atmosphere.

ides based on MMCA, API and various amounts of SBA-15 and Table I summarizes the results. It is noted that the incorporation of mesoporous silica increased the thermal stability of the polyimides up to a content of 7 wt%, due to the enhanced interaction between the polyimide matrix and mesoporous silica[19] as well as the inherently good thermal stability of inorganic silica.[20] However, as the amount of SBA-15 is increased i.e. to 10 wt% and 15 wt%, the thermal stability decreased owing to the phase separation between the compounds, as clearly inferred from their SEM images. The degradation curve showed a rapid 5% weight loss that can be attributed to the loss of water trapped in the mesopores and/or condensation of the silanol groups (Si-OH), which became more evident as the amount of SBA-15 increased. All of the hybrid composites showed a residual weight at around 600 °C owing to the $SiO_2$ ash that remained, with the amount of residual ash increasing in proportion to the amount of SBA-15 inside the hybrid composites, suggesting the successful incorporation of higher amounts of silica.[21]

Figure 8 illustrates the variation of $T_g$ of the polyimide hybrid composites based on BOCA and MMCA with different compositions and Table I summarizes the results. API exhibited $T_g$ around 241 °C.[8] The $T_g$ of the hybrid composites showed a maximum and then decreased as the amount of SBA-15 increased. The increase in $T_g$ can be explained in terms of the restricted motions of the polymer chains in the presence of the silica network, due to the efficient phase miscibility, as shown in the SEM images,[22] while the decrease

**Table I. Summary of the Properties of the Fully Aliphatic Polyimide/Mesoporous Silica Hybrid Composites**

| Sample Name | Diamine | Weight % of SBA-15 | $T_g$ (°C) | $T_d$ (°C) | | Dielectric Constant ($\varepsilon$) |
|---|---|---|---|---|---|---|
| | | | | 5% wt loss | 10% wt loss | |
| API | MMCA | 0 | 241 | 326 | 364 | 2.57 |
| $API_{(3)}$ | MMCA | 3 | 263 | 420 | 436 | 2.56 |
| $API_{(5)}$ | MMCA | 5 | 288 | 426 | 438 | 2.51 |
| $API_{(7)}$ | MMCA | 7 | 309 | 431 | 444 | 2.50 |
| $API_{(10)}$ | MMCA | 10 | 258 | 389 | 435 | 2.56 |
| $API_{(15)}$ | MMCA | 15 | 234 | 308 | 430 | 2.70 |

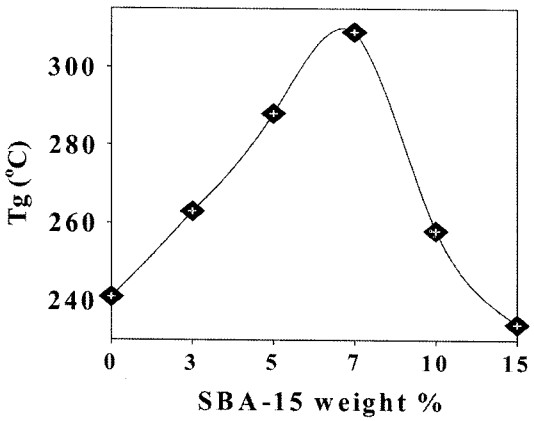


**Figure 8.** Variation in the glass transition temperature of the API/SBA-15 hybrid composites with the amount of SBA-15.

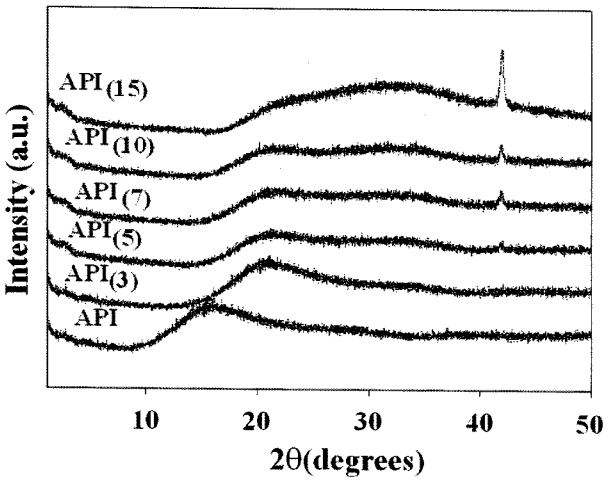


**Figure 9.** WAXD patterns of API/SBA-15 hybrid composites.

of $T_g$ can be attributed to the plasticizing effect of the mesoporous silica, due to its mesoporosity, which plays an increasingly prominent role as the amount of SBA-15 increases.[9]

**WAXD Studies.** Figure 9 displays the representative WAXD results. The neat polyimides exhibited peaks combined with an amorphous halo in the region of $2\theta < 20°$, indicating their intermolecular regularity. The major peak shows a clear split as the mesoporous silica content increases, with the major scattering peak at $2\theta = 17\text{-}30°$ and the weak peak at $2\theta = 20\text{-}40°$. The incorporation of SBA-15 also resulted in a shift towards a higher scattering angle, a lowering of the peak intensity and broadening of the peaks. This trend can be attributed to the decrease in the scattering intensity, disruption of the internal order and increase of the lattice strain.[23] The broad peak is due to the scattering associated with the short range order of the polymer chains within the SBA framework combined with the amorphous halo. The shift to higher scattering angles, for the hybrid composites with up to 7 wt% of SBA-15, implies the formation of the nanometer scale structure of SBA-15, i.e. the formation of nanohybrid composites. However, there was no shift in the scattering angle when the amount of SBA-15 was higher than 10 wt%, implying the existence of phase separation. The origin of the sharp peak at 20-40° is not clear at this moment, though it may be related to the microvoids within the SBA-15 (i.e. interference scattering due to the presence of voids).

**Trends in Dielectric Constant.** Fully aliphatic polyimides show a low dielectric constant ($\varepsilon$) due to their low hydrophobicity and polarity. It is also no doubt that mesoporous silica possesses a low $\varepsilon$ value due to its porous structure. Thus, the hybrid composites were expected to show low dielectric constants. According to the predictions using the Maxwell-Garnett equation (1), considering the hybrid composite films as a dual-component system consisting of API and SBA-15, it is believed that the reduction of the dielectric constant is due to the air voids ($\varepsilon = 1$) in the mesoporous silica.[24]

$$\varepsilon_e = \varepsilon \frac{\varepsilon_m(1+2\delta) - \varepsilon_i(2\delta-2)}{\varepsilon_i(2+\delta) + \varepsilon_m(1-\delta)} \quad (1)$$

where $\varepsilon_e$, $\varepsilon_i$ and $\varepsilon_m$ are the effective dielectric constants of the medium, the inclusions (SBA-15 in our study) and the matrix (API in our study), respectively, and $\delta$ is the volume fraction of the embedded material (SBA-15).

So according to the theoretical data, the $\varepsilon$ values should decrease continuously with increasing amount of SBA-15. Table I shows, however, that the measured values present a minimum at 7 wt% and then show a decrease. This implies that the reduction in the $\varepsilon$ values is not only due to the air volume stored within SBA-15. This result can be explained by applying Bruggeman's model (eq. (2)), assuming the existence of three phases in the hybrid composites, namely API, SBA-15 and air, which includes the total air volume within the mesoporous silica, as well as the total air volume in the hybrid composites. This is because the actual air volume in the hybrid composites is much higher than that in the mesoporous silica, due to the existence of air voids in the gaps of the interphase between the SBA-15 and PI matrix, together with the free volume created by the introduction of macro-sized domains.[25]

$$\delta_m\left(\frac{\varepsilon_m-\varepsilon_e}{\varepsilon_m+2\varepsilon_e}\right) + \delta_i\left(\frac{\varepsilon_i-\varepsilon_e}{\varepsilon_i+2\varepsilon_e}\right) + \delta_a\left(\frac{\varepsilon_a-\varepsilon_e}{\varepsilon_a+2\varepsilon_e}\right) = 0 \quad (2)$$

where $\varepsilon_e$, $\varepsilon_i$, $\varepsilon_m$ and $\varepsilon_a$ are the effective dielectric constants of the medium, the inclusions (SBA-15 in our study), the matrix (API in our study) and air, and $\delta_m$, $\delta_i$ and $\delta_a$ are the volume fractions of API, SBA-15 and air, respectively, in our study.

Therefore it can be concluded that the air volume stored in the mesoporous silica, the voids arising from the SBA-15/API interfacial gaps and the free volume generated by the macro-sized domains together contribute to the reduc-

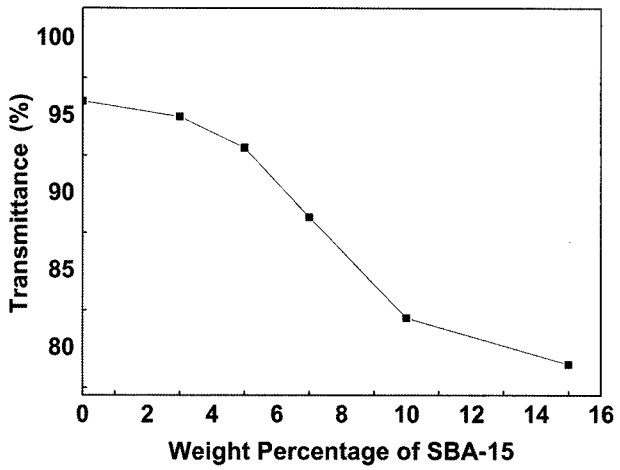


**Figure 10.** Optical transparency of polyimides with varying amount of SBA-15 under visible light at 500 nm.

tion of the dielectric constant. Moreover, the air volume in the pores created during the mixing process should also be added to the total air volume of the hybrid composites.[12] According to Bruggeman's model, this total air volume presents a maximum at a favorable optimum concentration of mesoporous silica and thereafter begins to decrease with increasing amount of the mesoporous material,[21] which tallies exactly with our findings. The incorporation of too much SBA-15 (i.e. 15 wt%) resulted in an increase in the $\varepsilon$ values beyond that of pure API, mainly due to the increase in the surface silanols on the pore walls of SBA-15 and the absorbed water inside the powders.[26]

**Transparency Measurements.** Figure 10 displays the optical properties of API as a function of the weight percentage of SBA-15 at 500 nm. The higher transparency of the fully aliphatic polyimides, owing to their low molecular density, polarity and lower probability of inter- and intra molecular charge transfer, makes them superior to aromatic polyimides. Though the hybrid composites exhibited low transparency, they still possess a marginal transparency of around 80% up to 10 wt% of SBA-15.

## Conclusions

In summary, we synthesized hybrid composites based on fully aliphatic polyimides using the alicyclic dianhydride, BOCA, the diamines, MMCA, and the mesoporous silica, SBA-15. The resulting materials showed interesting thermo-optical and dielectric properties, which were tunable by varying the amount of SBA-15 added. We found that when the amount of SBA-15 is 7 wt% in the aliphatic polyimide matrix the hybrid composites showed optimal conditions; i.e. maximum $T_g$ value of 309 °C with 10% weight loss at around 444 °C, respectively. Also, the hybrid composites having 7 wt% of SBA-15 exhibited minimum dielectric constant of 2.50, with marginal transparencies of more than 85%. These materials are promising hybrid composites for future microelectronic and optoelectronic applications.

**Acknowledgements.** This work was supported by a grant from the Fundamental R&D Program for Core Technology of Materials funded by the Ministry of Knowledge Economy, Republic of Korea, Korea Science and Engineering Foundation (KOSEF) through the Acceleration Research Program funded by the Ministry of Education, Science and Technology (MEST; No. 2009-0078791), the WCU program of MEST (No. R32-2008-000-10174-0), and the Brain Korea 21 Project. We also thank the Pohang Accelerator Laboratory, Korea for SAXS measurements.

## References

(1) R. I. Nooney, D. Thirunavukkarasu, Y. Chen, R. Josephs, and A. E. Ostafin, *Chem. Mater.*, **14**, 4721 (2002).
(2) C. E. Fowler, D. Khushalani, B. Lebeau, and S. Mann, *Adv. Mat.*, **13**, 649 (2001).
(3) A. Y. Khodakov, V. L. Zholobenko, R. Bechara, and D. Durand, *Micropor. Mesopor. Mater.*, **79**, 29 (2005).
(4) L. Qingyi, G. Feng, K. Sridhar, and E. M. Thomas, *J. Am. Chem. Soc.*, **126**, 8650 (2004).
(5) M. Can, B. Akça, A. Yilmaz, and D. Üner, *Turk. J. Phys.*, **29**, 287 (2005).
(6) D. Zhao, J. Feng, Q. Huo, N. Melosh, G. H. Fredrickson, and B. F. Chmelka, *Science*, **279**, 548 (1998).
(7) J. Y. Lee, J. H. Kim, and B. K. Rhee, *Macromol. Res.*, **15**, 234 (2007).
(8) A. S. Mathews, I. Kim, and C. S. Ha, *J. Appl. Polym. Sci.*, **102**, 3316 (2006).
(9) A. S. Mathews, I. Kim, and C. S. Ha, *J. Polym. Sci. Part A: Polym. Chem.*, **44**, 5254 (2006).
(10) A. S. Mathews, I. Kim, and C. S. Ha, *Macromol. Res.*, **15**, 114 (2007).
(11) J. Yang and M. H. Lee, *Macromol. Res.*, **12**, 263 (2004).
(12) T. Lee, S .S. Park, Y. Jung, S. Han, D. Han, I. Kim, and C. S. Ha, *Eur. Polym. J.*, **45**, 19 (2009).
(13) W. Guo, J. Y. Park, M. O. Oh, H. W. Jeong, W. J. Cho, I. Kim, and C. S. Ha, *Chem. Mater.*, **15**, 2295 (2003).
(14) (a) D. Zhao, J. Feng, Q. Huo, N. Melosh, G. H. Fredrickson, B. F. Chmelka, and G. D. Stucky, *Science*, **279**, 548 (1998). (b) J. Yoon, K. W. Kim, J. Kim, K. Heo, K. S. Jin, S. Jin, T. J. Shin, B. Lee, Y. Rho, B. Ahn, and M. Ree, *Macromol. Res.*, **16**, 275 (2008).
(15) S. Brunauer, L. Deming, W. Deming, and E. Teller, *J. Am. Chem. Soc.*, **62**, 1723 (1940).
(16) Y. F. Shi, Y. Meng, D. H. Chen, S. J. Cheng, P. Chen, H. F. Yang, Y. Wan, and D. Zhao, *Adv. Funct. Mater.*, **16**, 561 (2006).
(17) Y. Kim, K. Han, and C. S. Ha, *Macromolecules*, **35**, 8759 (2002).
(18) Y. Watanabe, Y. Sakai, M. Ueda, Y. Oishi, and K. Mori, *Chem. Lett.*, **29**, 450 (2000).
(19) K.G. Sharp, *Adv. Mater.*, **10**, 1243 (1998).

(20) J. Y. Wen and G. L. Wilkes, *Chem. Mater.*, **8**, 1667 (1996).
(21) J. Lin and X. Wang, *Polymer*, **48**, 318 (2007).
(22) C. F. Chen, H. H. Cheng, P. W. Cheng, and Y. J. Lee, *Macromolecules*, **39**, 7583 (2006).
(23) C. Suryanarayanan and M. G. Norton, *X-Ray Diffraction: A Practical Approach*, Plenum, New York, 1998, Chapter 3, p 80.
(24) T. J. Hernandez and G. A. Mendoza, *J. Non-Cryst. Solids*, **351**, 2029 (2005).
(25) M. A. Wahab, I. Kim, and C. S. Ha, *Polymer*, **44**, 4705 (2003).
(26) C. K. Min, T. B. Wu, W. T. Yang, and C. L. Chen, *Compos. Sci. Tech.*, **68**, 1570 (2008).